AGU PUBLICATIONS

Paleoceanography

RESEARCH ARTICLE
10.1002/2014PA002727

Key Points:
- Subduction depth of AAIW-depth varies on glacial/interglacial timescales
- Shoaling of AAIW leads to an expansion of UCDW
- UCDW shoaling enlarges the glacial carbon pool

Supporting Information:
- Text S1 and Tables S1–S2
- Figure S1
- Figure S2

Correspondence to:
T. A. Ronge,
Thomas.Ronge@awi.de

Citation:
Ronge, T. A., S. Steph, R. Tiedemann, M. Prange, U. Merkel, D. Nürnberg, and G. Kuhn (2015), Pushing the boundaries: Glacial/interglacial variability of intermediate and deep waters in the southwest Pacific over the last 350,000 years, *Paleoceanography*, *30*, 23–38, doi:10.1002/2014PA002727.

Received 25 SEP 2014
Accepted 13 JAN 2015
Accepted article online 16 JAN 2015
Published online 11 FEB 2015

Pushing the boundaries: Glacial/interglacial variability of intermediate and deep waters in the southwest Pacific over the last 350,000 years

Thomas A. Ronge[1], Silke Steph[1], Ralf Tiedemann[1], Matthias Prange[2], Ute Merkel[2], Dirk Nürnberg[3], and Gerhard Kuhn[1]

[1]Alfred Wegener Institute Helmholtz Center for Polar and Marine Research, Bremerhaven, Germany, [2]MARUM and Geoscience Department, University of Bremen, Bremen, Germany, [3]GEOMAR Helmholtz Center for Ocean Research, Kiel, Germany

Abstract Glacial/interglacial changes in Southern Ocean's air-sea gas exchange have been considered as important mechanisms contributing to the glacial/interglacial variability in atmospheric CO_2. Hence, understanding past variability in Southern Ocean intermediate to deep water chemistry and circulation is fundamental to constrain the role of these processes on modulating glacial/interglacial changes in the global carbon cycle. Our study focused on the glacial/interglacial variability in the vertical extent of southwest Pacific Antarctic Intermediate Water (AAIW). We compared carbon and oxygen isotope records from epibenthic foraminifera of sediment cores bathed in modern AAIW and Upper Circumpolar Deep Water (UCDW; 943–2066 m water depth) to monitor changes in water mass circulation spanning the past 350,000 years. We propose that pronounced freshwater input by melting sea ice into the glacial AAIW significantly hampered the downward expansion of southwest Pacific AAIW, consistent with climate model results for the Last Glacial Maximum. This process led to a pronounced upward displacement of the AAIW-UCDW interface during colder climate conditions and therefore to an expansion of the glacial carbon pool.

1. Introduction

Surrounding Antarctica, the Southern Ocean (SO) plays a vital role in the global overturning circulation as it connects the Pacific, Atlantic, and Indian Oceans. The transport of Antarctic Intermediate Water (AAIW) in particular is crucial for the redistribution of nutrients, heat, and freshwater within the global ocean [*Schmitz*, 1995; *Toggweiler et al.*, 1991]. On glacial/interglacial timescales, climate signals of upwelled deep water were transported from the Southern Ocean toward the major ocean basins within the AAIW [*Basak et al.*, 2010; *Bryan et al.*, 2010; *Marchitto et al.*, 2007; *Stott et al.*, 2009] and, at least during the last deglacial, AAIW was an important indicator for the transport of CO_2 from old deep water masses to the atmosphere [e.g., *Marchitto et al.*, 2007; *Rose et al.*, 2010]. Today, most of the anthropogenic CO_2 entering the ocean depths is contained within AAIW [*Downes et al.*, 2010; *Murata et al.*, 2007, 2010; *Sabine et al.*, 2004]. The importance of the oceanic uptake of CO_2 (not only via AAIW) becomes evident by the fact that without this process, the atmospheric CO_2 concentration would be about 55 ppm higher than it is today (~400 ppm) [*Sabine et al.*, 2004]. Despite the importance of AAIW for the global climate, especially in view of the current climate change, only scarce information about the temporal changes in its vertical and lateral expansion exists. In this study, we present new epibenthic $\delta^{13}C$ and $\delta^{18}O$ records from the Chatham Rise and the Tasman Sea off New Zealand that span the last 350 kyr. In comparison to a previously published record from sediment core MD97-2120 (1210 m; 45°32′S 174°55′E) [*Pahnke and Zahn*, 2005] we are able to constrain the vertical extent of AAIW over different climatic cycles by using isotope records from multiple sediment cores from different water depths.

1.1. Regional Oceanography

Dominating the SO, the Antarctic Circumpolar Current (ACC) is propelled by strong Southern Hemisphere Westerly Winds (SWW) [*Rintoul et al.*, 2001]. In our research area, the New Zealand microcontinent is significantly affecting the position of the ACC's northern boundary, the Subantarctic Front (SAF) [*Carter and Wilkin*, 1999]. South of New Zealand the Macquarie Ridge and the Campbell Plateau (Figure 1) dictate the location of the SAF [*Heath*, 1981]. Likewise, the northern edge of the SO, namely, the Subtropical Front (STF) is

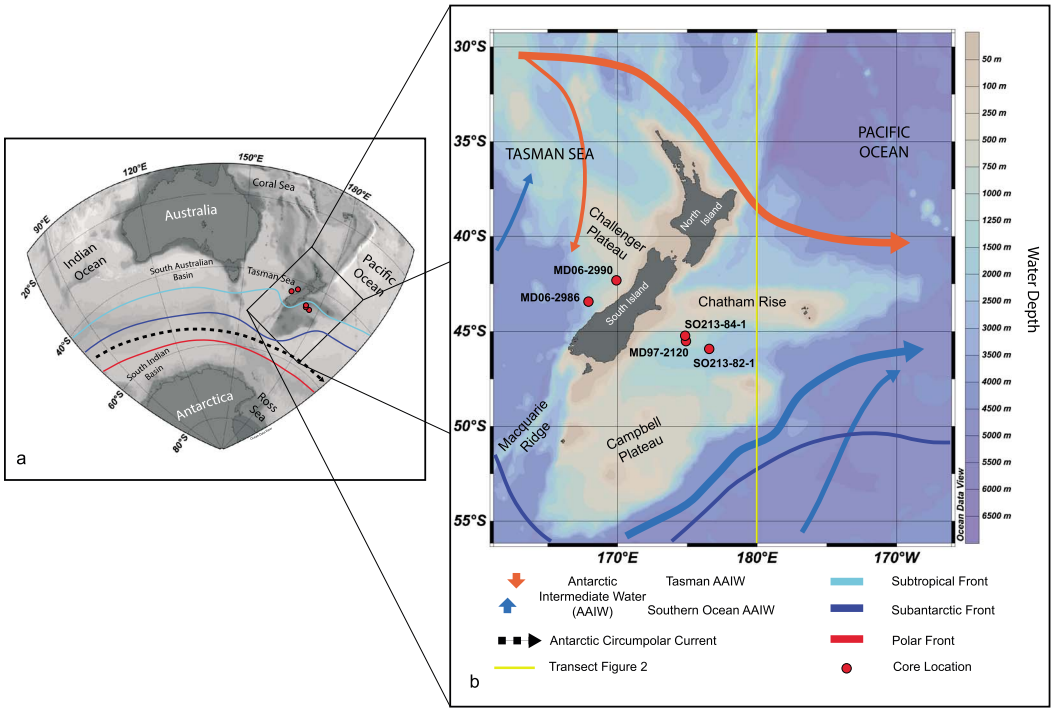

Figure 1. Bathymetric and oceanographic map of the study area showing the major oceanic fronts and current systems in the Southern Ocean. (a) Supraregional overview map of the SW Pacific and Indian sector of the Southern Ocean. (b) Regional setting of the New Zealand subcontinent [*After Orsi et al.*, 1995; *Bostock et al.*, 2013a; *Bostock et al.*, 2013b].

forced to follow the continental shelf of the submerged microcontinent and is topographically restricted by the submerged Chatham Rise (Figure 1b) [*Crundwell et al.,* 2008; *Heath*, 1981; *Sutton*, 2003].

The subsurface southwest Pacific is subdivided into four major water masses. Subantarctic Mode Water (~300–800 m) [*Crundwell et al.,* 2008] is characterized by its uniform temperature (8–9°C) and high oxygen concentrations. In winter, Subantarctic Mode Water is formed via the process of deep mixing along the SAF [*Bostock et al.,* 2013a; *McCartney*, 1977]. Further down, Antarctic Intermediate Water (AAIW) expands the prominent salinity minimum into a depth between 800 and 1450 m (Figure 2) [*Hayward et al.,* 2002; *Heath*, 1985; *McCartney*, 1977; *Sloyan et al.,* 2010]. South of the Chatham Rise, in our research area, intermediate waters originate directly from the ACC [*Hayward et al.,* 2002]. Intermediate waters to the north of the Chatham Rise are modified by the admixture of waters from the Coral and Tasman Seas [*Bostock et al.,* 2013a; *Tomczak and Godfrey*, 1994]. *Bostock et al.* [2013b] refer to the intermediate waters, formed in a small region close to the SAF off New Zealand as Southern Ocean AAIW. This SO AAIW forms directly from upwelled nutrient- and CO_2-rich Circumpolar Deep Water (CDW). Accordingly, the chemical signature of AAIW carries information about the efficiency of the biological pump and air-sea gas exchange [*Sigman et al.,* 2010]. Simplified, the remaining nutrient concentration of sinking AAIW is a measure of the difference of upwelled nutrients and biological consumption in the uppermost water column, while the overturning intensity is modified by the strength of the wind-induced upwelling. The associated processes within this loop from upwelling to sinking are crucial for the oceanic release or uptake of atmospheric CO_2. Below the AAIW, CDW as the most voluminous SO water mass [*Carter et al.,* 2009] is subdivided into two distinctive water masses. Upper CDW (UCDW; ~1450–2900 m) outcrops around Antarctica and is defined by an oxygen minimum that is formed by the influence of old deep waters from the North Pacific and Indian Oceans [*Callahan*, 1972; *Carter et al.,* 2009]. Increased salinity by the entrainment of North Atlantic Deep Water marks the Lower CDW (LCDW; ~2900–4500 m) [*Callahan*, 1972; *Orsi et al.,* 1995]. Below ~3900 m, LCDW is influenced by cold Antarctic Bottom Waters [*Bostock et al.,* 2013a]. According to *McCave and Carter* [1997], the majority of deep water (>2000 m) entering the Pacific Ocean is transported via a strong deep western boundary current (DWBC) southeast of New Zealand. Moving a volume of about 20 Sv, the Pacific DWBC is one of the strongest boundary currents worldwide [*Schmitz*, 1995].

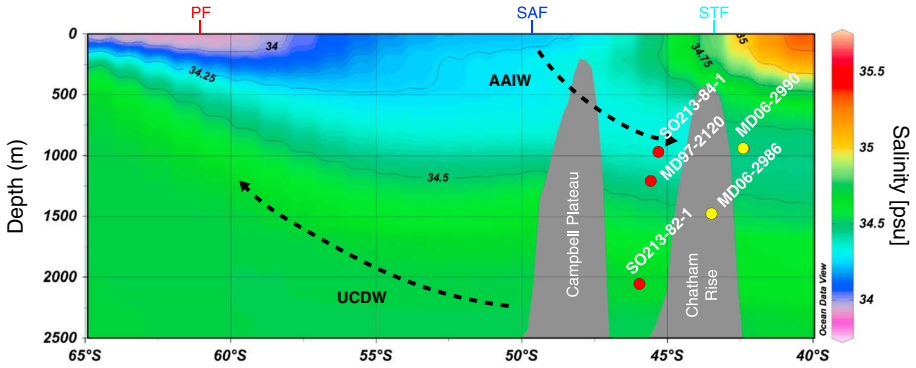

Figure 2. Salinity section along the 180° meridian (indicated in Figure 1b; WOA; [*Antonov et al.*, 2010]). To project the analyzed sediment cores (red dots = Bounty Trough and yellow dots = Tasman Sea) in this section, their longitudes were adjusted to 180°. Arrows indicate the prevailing current regime of SW Pacific water masses. AAIW = Antarctic Intermediate Water, UCDW = Upper Circumpolar Deep Water, PF = Polar Front, SAF = Subantarctic Front, and STF = Subtropical Front.

2. Material and Methods

We analyzed four sediment cores from the Tasman Sea and the Bounty Trough off New Zealand, collected during R/V *Marion Dufresne* MD152 and R/V *Sonne* SO213/2 cruises in 2006 and 2011, respectively [*Proust et al.,* 2006; *Tiedemann*, 2012]. Cores MD06-2990 (943 m; 42°19′S 169°55′E) and MD06-2986 (1477 m; 43°27′S 167°54′E) were collected in the Tasman Sea west of New Zealand. Cores SO213-84-1 (972 m; 45°07′S 174°34′E) and SO213-82-1 (2066 m; 45°46′S 176°36′E) are located on the eastern side of the island, in the Bounty Trough south of the Chatham Rise. Today, SO213-84-1 and MD06-2990 are bathed by AAIW, MD06-2986, and SO213-82-1 by Upper Circumpolar Deep Water (UCDW). The uppermost part of MD06-2990 was significantly disturbed during core recovery. We therefore used the top section of R/V *Sonne* core SO136-003 (42°17.74′S/169°52.66′E; 958 m water depth) [*Thiede*, 1999] to replace the affected sediment sequence (see description of the age model for additional information). Sediment core SO213-82-1 yields an average sedimentation rate of 3 cm/kyr, SO213-84-1 shows a sedimentation rate of 6 cm/kyr while MD06-2986 and MD06-2990 yield sedimentation rates of 8 cm/kyr and 3 cm/kyr, respectively. The working halves of both SO213 cores were sampled at 2 cm intervals. The top 13.50 m of core MD06-2990 (33.55 m length) and the top 2.50 m of core SO136-003 were sampled at 2 cm intervals, core MD06-2986 (32.68 m length) was sampled at 4 cm intervals. Subsequently, the samples were frozen and freeze dried for 2 to 3 days, depending on the samples' water content. After freeze drying, the samples were wet sieved through a sieve with a mesh size of 63μm and dried for two days at ~50°C. When dry, the samples were fractionated through different mesh sieves (125 μm, 250 μm, 315 μm, and 400 μm). The foraminifera were picked from the size fractions 250–315 μm and 315–400 μm using a reflective light microscope with a fiftyfold magnification.

2.1. Stable Isotopes

Isotope ratios (reported in delta notation versus VPDB calibrated via international standard NBS19) of δ^{13}C and δ^{18}O were measured on four specimens of *Cibicidoides wuellerstorfi* or on three specimens of *Uvigerina peregrina,* in samples lacking a sufficient amount of *C. wuellerstorfi*. All measurements were conducted at the Alfred Wegener Institute in Bremerhaven, using a Finnigan MAT 253 mass spectrometer with a Kiel IV Carbonate Device. The long-term precision based on an internal laboratory standard (Solnhofen limestone) measured over a 1 year period together with samples was better than ±0.06‰ for δ^{13}C and ±0.08‰ for δ^{18}O.

C. wuellerstorfi was present throughout all sediment cores. However, in a few intervals we used *U. peregrina*, where *C. wuellerstorfi* was absent (Figure S1 in the supporting information).

2.1.1. Oxygen Isotopes

Primarily, we used the benthic δ^{18}O signal for the development of our age models. In addition to changes in global ice volume [*Shackleton*, 1977], which provide the stratigraphic basis in our study, the benthic δ^{18}O signal reflects variations in local temperature and/or salinity [*Emiliani*, 1955; *Epstein and Mayeda*, 1953]. In general, the δ^{18}O values recorded by *C. wuellerstorfi* deviate by ~0.64‰ from *U. peregrina* values [*Shackleton and Opdyke*, 1973].

The $\delta^{18}O_{Cib\ \&\ Uvi}$ values in the records of SO213-84-1 and SO213-82-1 show a very high correlation with a mean offset *C. wuellerstorfi-U. peregrina* of 0.48‰. Therefore, we used this offset of 0.48‰ to correct the Bounty Trough $\delta^{18}O$ values of *C. wuellerstorfi* for species-specific fractionation [*McCave et al.,* 2008; *Pahnke and Zahn*, 2005] instead of using an offset of 0.64‰ [*Duplessy et al.,* 1988; *Shackleton and Opdyke*, 1973]. However, the Tasman Sea records MD09-2986 and MD06-2990/SO136-003 show a good correlation with an offset of 0.64‰ and were therefore rendered to Uvi-equivalent by adding 0.64‰, according to the accepted method [*Shackleton and Opdyke*, 1973].

2.1.2. Carbon Isotopes

In paleoceanography, the epibenthic $\delta^{13}C$ records of the foraminifer *C. wuellerstorfi* are commonly used as a proxy for changes in water mass nutrient concentrations [*Kroopnick*, 1985; *Zahn et al.,* 1991]. The $\delta^{13}C$ values in the water column strongly depend on the remineralization of ^{12}C-enriched organic matter, which leads to the consumption of oxygen and the release of nutrients. Low $\delta^{13}C$ values are therefore indicative of high-nutrient concentrations and weakly ventilated water masses. Furthermore, oceanic $\delta^{13}C$ values are influenced by the release of terrestrial carbon during glacial times [*Peterson et al.,* 2014] as well as by thermodynamic [*Broecker and Maier-Reimer*, 1992] and biological effects [*Farquhar et al.,* 1989].

As described above, we used *U. peregrina* to fill the intervals barren of *C. wuellerstorfi*. Following the methods of *Pahnke and Zahn* [2005] and *McCave et al.* [2008], we disregarded the usual +0.9‰ *U. peregrina* to *C. wuellerstorfi* offset. As these authors showed, the epifaunal to infaunal $\delta^{13}C$ difference off New Zealand is far from constant but varies on glacial to interglacial timescales as a function of $\delta^{18}O_{Uvi}$. Over the whole record, the average offset $\Delta\delta^{13}C_{Cib\text{-}Uvi}$ is 0.81‰ and therefore close to the offset of 0.9‰. However, the addition of 0.9‰ proves to be impractical for the conversion of $\delta^{13}C_{Uvi}$ in SO213-82-1, if just the epifaunal to infaunal offsets of the Holocene and the Last Glacial Maximum (LGM) are compared. During the Holocene, the mean $\Delta\delta^{13}C_{Cib\text{-}Uvi}$ of SO213-82-1 is as high as 1.09‰ while the LGM offset is only 0.47‰. To account for this variable offset, we used the regression equation of *McCave et al.* [2008]:

$$\Delta\delta^{13}C_{Cib-Uvi} = 0.464\delta^{18}O_{Uvi} - 2.753 \quad (r = 0.629;\ \ n = 57)$$

A comparison of raw isotopic data to the corrected values of SO213-82-1 is shown in Figure S1.

2.2. Paleoproductivity Calculations

In order to assess the influence of phytodetritus (high in ^{12}C) on the benthic $\delta^{13}C$ signals [*Mackensen et al.,* 2001], we calculated the paleoproductivity for sediment cores SO213-82-1 and SO213-84-1 (Bounty Trough). Physical properties were measured with a spacing of 10 cm, using a PC controlled Eltra CS-2000 Carbon Sulfur element analyzer. We reconstructed the paleoproductivity (PP; $gC/m^2/yr$) according to *Stein* [1991]:

$$PP = 5.31\ \ \left(C_{org}(DBD)\right)^{0.71} \times LSR^{0.07}DEP^{0.45}$$

DBD is the dry bulk density, C_{org} (%) is the content of organic carbon, LSR is the linear sedimentation rate ($cm\ kyr^{-1}$), and DEP is the sediment cores water depth.

2.3. Age Determination

Our age models reflect a combination of radiocarbon dating and $\delta^{18}O$ correlation to age scaled reference records. The age model for the upper section of cores MD06-2986 and MD06-2990/SO136-003, SO213-82-1, and SO213-84-1 is based on Accelerator Mass Spectrometry (AMS) ^{14}C dates. AMS ^{14}C dating was performed on mixed planktic foraminifera (MD06-2986, eight samples; Table S1), on *Globorotalia inflata* (SO136-003, six samples; Table S1) or on *Globigerina bulloides* (SO213-82-1, seven samples; SO213-84-1, three samples). The samples were prepared and analyzed in the Leibniz-Laboratory for Radiometric Dating and Isotope Research at the Christian-Albrechts-University of Kiel (MD06-2986), at the AMS ^{14}C Laboratory at the Eidgenössische Technische Hochschule Zürich (SO136-003) and at the NOSAMS facility in Woods Hole, USA (SO213-82-1 and SO213-84-1). AMS ^{14}C ages were converted to calendar ages using CALIB 7.0 of M. Stuiver et al. (2014, CALIB 7.0. WWW program and documentation), applying a local reservoir correction of 640 years for interglacial and 1970 years for glacial age [*Pahnke and Zahn*, 2005; *Sikes et al.,* 2000]. Beyond the range of radiocarbon dating, the age scale for our cores was obtained by correlating the oxygen isotope records (mainly indicative of changes in globalice volume) with the EPICA Dome C ice core (EDC) δD record on the AICC2012 timescale [*Bazin et al.,* 2013; *Jouzel et al.,* 2007; *Veres et al.,* 2013] (Figure 3). To guarantee the best possible correlation, we updated the MD97-2120 age model of *Pahnke and Zahn* [2005] to the EDC ice core

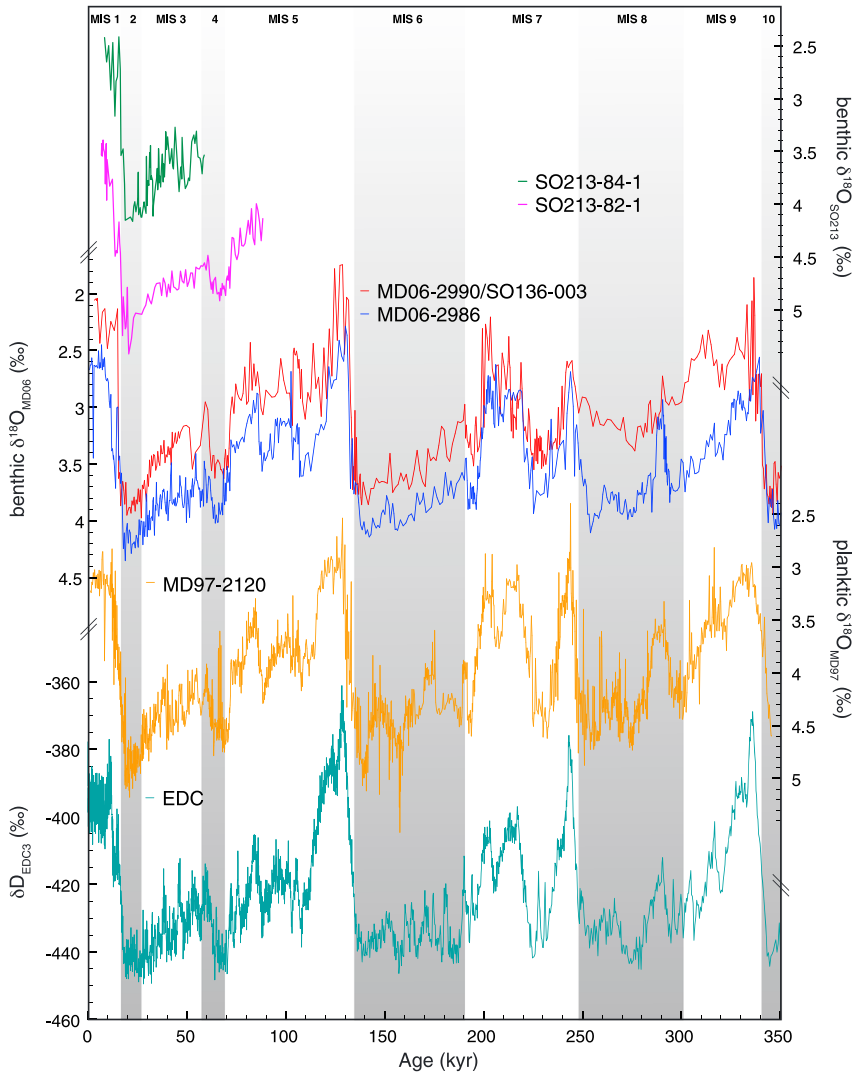

Figure 3. Benthic δ^{18}O isotope records measured on *C. wuellerstorfi*. Bounty Trough sediment cores SO213-82-1 (pink) and SO213-84-1 (green); Tasman sea records MD06-2986 (blue) and MD06-2990 (red). Isotope record of MD97-2120 (orange; [*Pahnke and Zahn*, 2005]) was measured on the planktic species *G. bulloides*. EPICA dome C δD-curve on the AICC2012 timescale (teal) [*Bazin et al.*, 2013; *Jouzel et al.*, 2007; *Veres et al.*, 2013]. Marine Isotope Stages: MIS 1 to MIS 10. Grey shadings indicate glacial stages.

and correlated our isotope records in the following to MD97-2120. Furthermore, we combined the benthic δ^{18}O records for cores SO136-003 and MD06-2990. The uppermost part, comprising the interval of Marine Isotope Stage (MIS) 1 to MIS 4 (0–65 kyr), is based on SO136-003, while the record below, down to 350 kyr (MIS 4 to MIS 10) is based on MD06-2990. Tuning our benthic δ^{18}O records to the EDC δD record resulted in a generally good agreement with the previously published benthic δ^{18}O record of core MD97-2120, collected from 1200 m water depth on Chatham Rise east of New Zealand (Figure 3) [*Pahnke and Zahn*, 2005].

2.4. Climate Modeling

In order to test hypothesized mechanisms that may have affected the characteristics and distribution of AAIW during glacial climates, we analyzed results from a glacial climate simulation using the Community Climate System Model version 3 (CCSM3). CCSM3 is a state-of-the-art fully coupled global general circulation model which is composed of four components representing the atmosphere, the ocean, the land surface, and sea ice [*Collins et al.,* 2006]. For the simulation in this study, the atmosphere model has a resolution of ~3.75° (T31 spectral truncation) with a vertical discretization of 26 levels, while the ocean and sea ice components are run on a nominal 3° grid with 25 levels in the ocean [*Yeager et al.,* 2006].

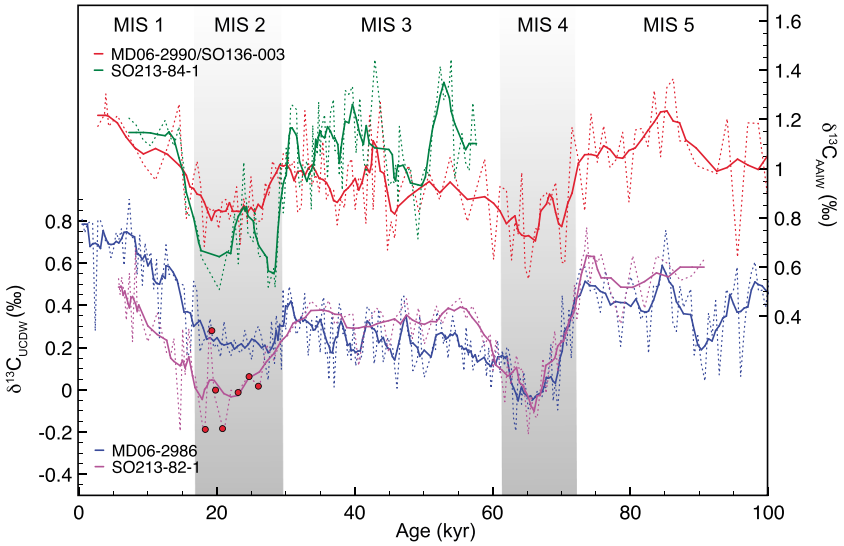

Figure 4. Comparison of Bounty Trough (SO213) and Tasman Sea (MD06) AAIW and UCDW benthic $\delta^{13}C$ (*C. wuellerstorfi*) records. Red dots indicate samples where *U. peregrina* was measured and transformed to *C. wuellerstorfi* equivalent according to *McCave et al.* [2008]. Throughout the whole time interval MD06-2986 (blue) and SO213-82-1 (pink) are bathed by UCDW, while MD06-2990/SO136-003 (red) and SO213-84-1 (green) are bathed by AAIW. Bold lines (five-point running average); stippled lines (raw data). Grey shadings as shown in Figure 3. The pronounced offset of SO213-82-1 and MD06-2986 during MIS 2 might derive from the use of *U. peregrina* in SO213-82-1 in this time interval.

Besides a preindustrial control run, a simulation of the LGM has been carried out [*Merkel et al.,* 2010]. This simulation takes into account the orbital parameters, the greenhouse gas concentrations, and the ice-sheet distribution of the LGM (21 kyr before present). Moreover, a sea level lowering of 120 m has been taken into account by a modification of the land-sea distribution, which for instance, leads to closure of the Bering Strait. For details of the experimental setup and spin-up procedure to obtain statistical equilibrium climates, the reader is referred to *Merkel et al.* [2010].

3. Results

Here we present proxy records from the four sediment cores described in section 2, which are indicative of changes in intermediate and deep water circulation (benthic $\delta^{13}C$ and $\delta^{18}O$) and biogenic productivity (TOC_{AR}) in our study area. These records allow us to identify climate-driven variations in the vertical extent of AAIW and UCDW. The two Tasman Sea records MD06-2086 and MD06-2990 span at least the last four glacial/interglacial cycles from 0 to 350 kyr, while SO213-84-1 and SO213-82-1 form the Bounty Trough do not exceed the last 100 kyr.

The close correlation of the Bounty Trough and Tasman Sea isotopic records in both AAIW (Figure 4 (top)) and UCDW (Figure 4 (bottom)) enables us to compare the water masses on both sides of New Zealand (Figure 1b).

3.1. Benthic $\delta^{18}O$

Except for SO213-82-1, where occasional samples of *U. peregrina* had to be analyzed to complement the record in depths barren of *C. wuellerstorfi* (see section 2), benthic $\delta^{18}O$ records were measured on monospecific samples of *C. wuellerstorfi*.

All records display similar distinctive glacial-interglacial cycles. The variability of the epibenthic $\delta^{18}O$ ($\delta^{18}O_{Cw}$) signal in our sediment cores reflects to a large part changes in global ice volume [*Shackleton*, 1977]. Yet the fact that the glacial/interglacial $\delta^{18}O_{Cw}$ amplitudes of up to ~2 ‰ in all cores generally exceed the sea level-related mean ocean $\delta^{18}O$ change of 0.8 to 1.1‰ [e.g., *Waelbroeck et al.,* 2002] indicates that a relevant portion of the $\delta^{18}O_{Cw}$ signal can be attributed to changes in water temperature and/or salinity [*Emiliani*, 1955; *Epstein and Mayeda*, 1953]. Although the glacial/interglacial $\delta^{18}O_{Cw}$ amplitudes are very similar in our records, $\delta^{18}O_{Cw}$ at the shallow cores MD06-2990/SO136-003 (945 m) and SO213-84-1 (972 m) was generally less than at the deeper core sites MD06-2986 (1477 m) and SO213-82-1 (2066 m) during the last four glacial/interglacial cycles (average AAIW/UCDW $\delta^{18}O$ offset ~0.49‰). This pattern points to higher temperatures and/or lower

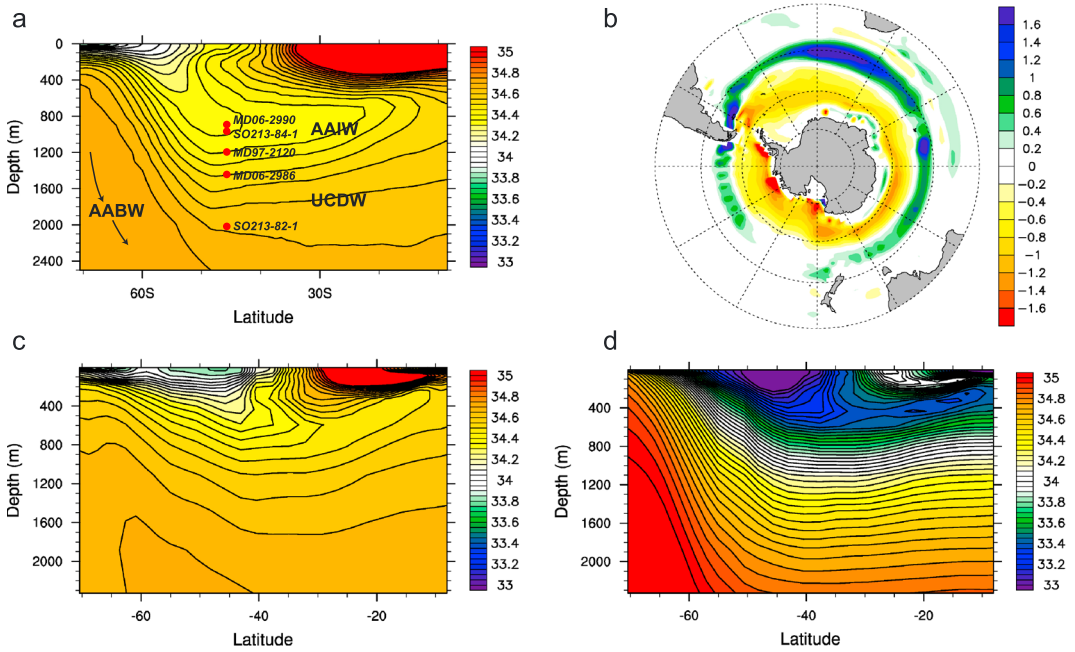

Figure 5. Pacific salinity distributions. (a) Observed present-day salinity, zonally averaged across the South Pacific (WOA) [*Antonov et al.*, 2010]. Red dots indicate the approximate water depth of sediment cores used in this study. (b) Modeled LGM Southern Ocean surface freshwater flux anomaly (m/yr; positive means freshwater flux into the ocean) relative to preindustrial (annual mean; 100 year average). (c) Modeled preindustrial salinity, zonally averaged across the South Pacific (annual mean; 100 year average). (d) As in Figure 5c but for the LGM (salinity adjusted such that global mean salinity is identical to preindustrial). AAIW = Antarctic Intermediate Water, UCDW = Upper Circumpolar Deep Water, and AABW = Antarctic Bottom Water.

salinity in the intermediate water (Figure 3). Because MD97-2120 shows the highest sedimentation rates (~16 cm/kyr; supplements of *Pahnke et al.* [2003b]) the pronounced amplitudes seen in the isotopic records could be ascribed to the high temporal resolution. Anyway, the proposed alternation of MD97-2120 between AAIW and UCDW that will be discussed below might also explain the high amplitudes of MD97-2120.

3.2. Benthic δ^{13}C

All sediment cores analyzed show similar δ^{13}C-patterns over the whole time interval, oscillating between glacial lows and interglacial highs, with a mean offset of ~0.7‰ between the AAIW and UCDW. The sediment cores bathed by modern AAIW (SO213-84-1 and MD06-2990) and by modern UCDW (SO213-82-1 and MD06-2986) show similar isotopic values of 1.14‰ for the AAIW and 0.4 to 0.6‰ for the UCDW (Table S2). Nevertheless, minor differences between Tasman Sea and Bounty Trough δ^{13}C values are evident especially during the last glacial (Figure 4). Throughout the LGM, the isotopic minima in Bounty Trough cores SO213-84-1 (AAIW) and SO213-82-1 (UCDW) are more pronounced than in their Tasman Sea counterparts. Therefore, we would like to mention that the δ^{13}C values of the respective time interval from core SO213-82-1 partly derive from adjusted *U. peregrina* values. Despite similar amplitudes in SO213-84-1 and SO213-82-1 a certain bias, introduced by the recalculation of *U. peregrina* values in SO213-82-1 cannot be completely excluded. In this context, it is noteworthy that the amplitudes for MIS 4 are nearly identical for SO213-82-1 and MD06-2986 with both records exclusively based on *C. wuellerstorfi* in this time interval (Figure 4).

3.3. Paleoproductivity

The PP for cores SO213-82-1 and SO213-84-1 amounts to a mean value of 55 gC/m^2/yr and ~53 gC/m^2/yr, respectively (Table S3). Consecutive glacials and interglacials show no prominent rise or drop in the PP (Table S3). Therefore, we detect no meaningful correlation between the changes in PP and δ^{13}C. In accordance to the results of *Mackensen et al.* [2001], we conclude that the δ^{13}C results measured on the epibenthic foraminifer species *C. wuellerstorfi* were not affected by the Phytodetritus Effect [*Mackensen et al.,* 1993].

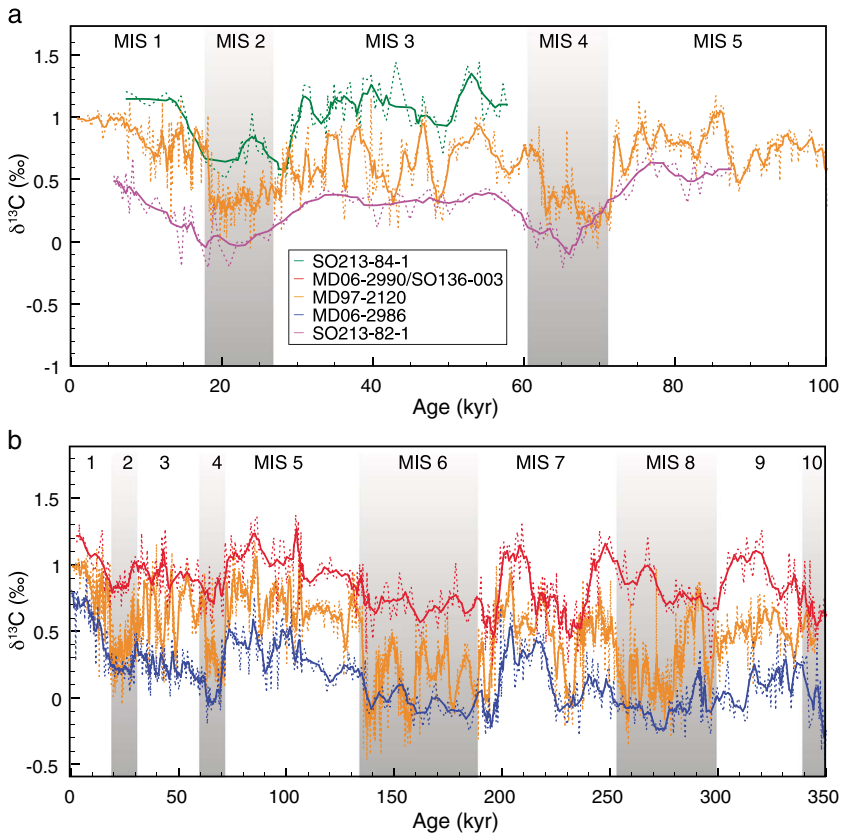

Figure 6. Comparison benthic carbon isotope records (*C. wuellerstorfi* equivalent) for the last (a) 100 kyr (Bounty Trough) and (b) 350 kyr (Tasman Sea) to the Bounty Trough record MD97-2120 [*Pahnke and Zahn*, 2005]. Bold lines (five-point running average); stippled lines (raw data).

3.4. Modeling Study

The overall distribution of South Pacific water masses with the characteristic low-salinity tongue of AAIW is clearly expressed in the preindustrial control simulation with the CCSM3 model (Figures 5a and 5c). Compared to observations, however, AAIW forms too far north which is likely related to simulated SWW that are biased toward the north [*Varma et al.,* 2011], a common shortcoming in most coarse-resolution climate models [e.g., *Rojas et al.,* 2009]. Moreover, the modeled AAIW is too shallow and too salty, despite a surface low-salinity bias south of ~40°S (Figures 5a and 5c). These model-data mismatches hamper direct geographical comparisons with proxy records from a specific location and imply that changes in the South Pacific hydrography are likely simulated somewhat too far north. Nevertheless, since the model captures the large-scale water masses relevant for this study, the model results are helpful in explaining glacial-interglacial changes of water mass characteristics and water mass distribution. In particular, enhanced surface freshwater input near the AAIW formation regions from melting sea ice in the LGM simulation (Figure 5b) leads to further freshening of the glacial AAIW (<33.5 psu) which spreads toward the north at a much shallower depth compared to the modern (Figure 5d).

4. Discussion

The most obvious result of our study is the constant offset of AAIW to UCDW δ^{13}C over the last 350 kyr, indicating no significant changes in water mass geometry. However, this interpretation is revealed as spurious by including another record bathed in modern AAIW-depth (MD97-2120; 1210 m) [*Pahnke and Zahn*, 2005], located between the other records used in this study, right at the boundary from AAIW to UCDW (Figure 2).

The pattern shown in Figure 2 locates the sediment cores MD06-2990/SO136-003 (943/958 m) and SO213-84-1 (972 m) close to the core of modern AAIW, today at about 700 m [*Heath*, 1985]. The deep water cores MD06-2986 (1477 m) and SO213-82-1 (2066 m) are located in UCDW. Despite the proximity of MD06-2986 to the interface of AAIW and UCDW (Figure 7), the very close correlation of $\delta^{13}C_{Cw}$ (Figure 4) with the

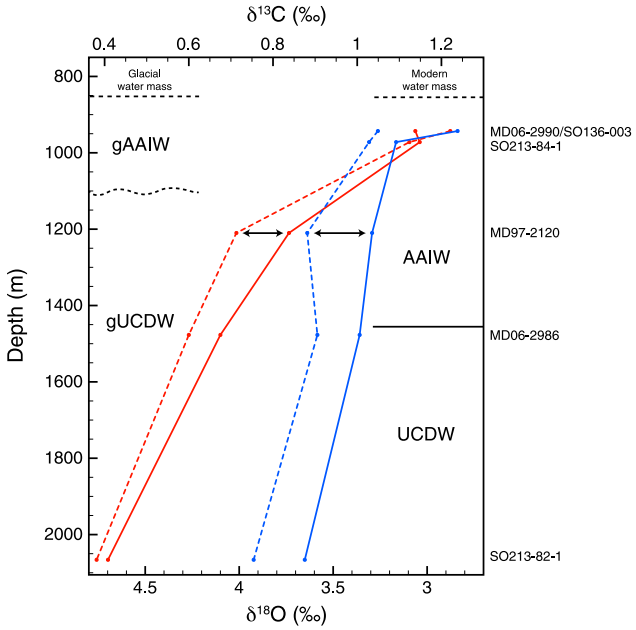

Figure 7. Comparison of averaged Holocene (solid lines) and LGM (dashed lines) benthic δ^{13}C (red) and δ^{18}O (blue) depth profiles. The glacial δ^{13}C values were corrected for the global isotopic shift by adding 0.38‰ [*Peterson et al.*, 2014]. Glacial δ^{18}O values were adjusted according to *Waelbroeck et al.* [2002] by subtracting 1.1‰. Black arrows indicate the pronounced isotopic shift in MD97-2120 caused by the shift from AAIW to UCDW. Glacial water mass distribution (gAAIW and gUCDW) as proposed in chapter 4; modern distribution after *Carter and McCave* [1997], *Hayward et al.* [2002], *Heath* [1985], and *Sloyan et al.* [2010]. Sediment cores (modern water depths) are indicated on the right axis.

deeper core SO213-82-1 illustrates that MD06-2986 remained in UCDW throughout the last 100 kyr (Figure 4). Therefore, we infer that this setup was maintained over the whole record of 350 kyr. This leaves MD97-2120 [*Pahnke and Zahn*, 2005] that also lies close to the boundary of AAIW and UCDW, in a crucial position for the investigation of the vertical AAIW extent through time.

During the LGM the $\delta^{13}C_{Cib}$ of AAIW (SO213-84-1 and MD06-2990/SO136-003) and UCDW (SO213-82-1 and MD06-2986) were lower by 0.34‰ and 0.42‰, respectively, than during the Holocene (Table S2). Thus, this difference fits to the mean whole-ocean δ^{13}C shift of 0.38±0.08‰ [*Peterson et al.*, 2014] and is clearly lower than the AAIW difference found by *Bostock et al.* [2010] of 0.8‰. Taking all cycles over the past 350 kyr into account, the isotopic offset between glacials and interglacials for MD06-2990/SO136-003 and MD06-2986 is 0.19‰ and 0.27‰, respectively. However, the LGM/Holocene offset of MD97-2120 is 0.53‰ and the 350 kyr average offset (MIS1–MIS9) is 0.41‰. Therefore, we argue that the pronounced depletion in glacial δ^{13}C of core MD97-2120 indicates an upward displacement of the AAIW-UCDW interface during glacial maxima. As it is shown in Table S2, the offset of MD97-2120 to MD06-2990/SO136-003 (943/958 m; AAIW) and MD06-2986 (1477 m; UCDW) is almost equal during interglacials, slightly leaning to the well-ventilated AAIW. However, during glacials the $\Delta\delta^{13}C_{2120\text{-}UCDW}$ decreases to only 0.18‰ while $\Delta\delta^{13}C_{AAIW\text{-}2120}$ increases to 0.54‰ (Table S2 and Figure 6).

Throughout the Holocene, the δ^{13}C values of MD97-2120 resemble those of SO213-84-1, yielding average values of 0.83‰ and 1.14‰, respectively (Figure 6). On the other hand, SO213-82-1 shows significantly lower values of 0.4‰. This pattern reflects the modern water mass distribution (Figure 7), locating MD97-2120 and SO213-84-1 in AAIW and SO213-82-1 in UCDW (Figure 2).

During the Last Glacial Maximum δ^{13}C of MD97-2120 approaches the values of SO213-82-1 (0.33‰ and 0‰, respectively). Even though the values of SO213-84-1 also decline, they remain at an average of 0.74‰ and thus considerably higher than the deeper cores. The deep water to intermediate water difference, $\Delta\delta^{13}C_{84\text{–}82}$ (0.74‰) remains similar to the Holocene offset of 0.74‰. Therefore, on a glacial/interglacial timescale, MD97-2120 appears to alternate between the water masses assigned to the sediment cores above and below, approaching the water mass interpreted as UCDW in glacial times. This pattern is particularly revealed in Figure 7 (black arrows), where the Glacial-to-Holocene offset in both, δ^{13}C and δ^{18}O of MD97-2120 is the largest from all sediment cores.

The pattern, with MD97-2120 δ^{13}C moving toward UCDW values during glacial maxima and toward AAIW during warmer periods, is repeated throughout the whole time interval analyzed (Table S2). We compared MD97-2120 to MD06-2990/SO136-003 and MD06-2986 on longer timescales, as both SO213 cores span only the last glacial to interglacial cycle (Figure 6). During the warmer stages 3, 5, 7, and 9, the average δ^{13}C values of the shallowest core MD06-2990/SO136-003 (interpreted as AAIW) are as high as 0.94‰, while MD97-2120

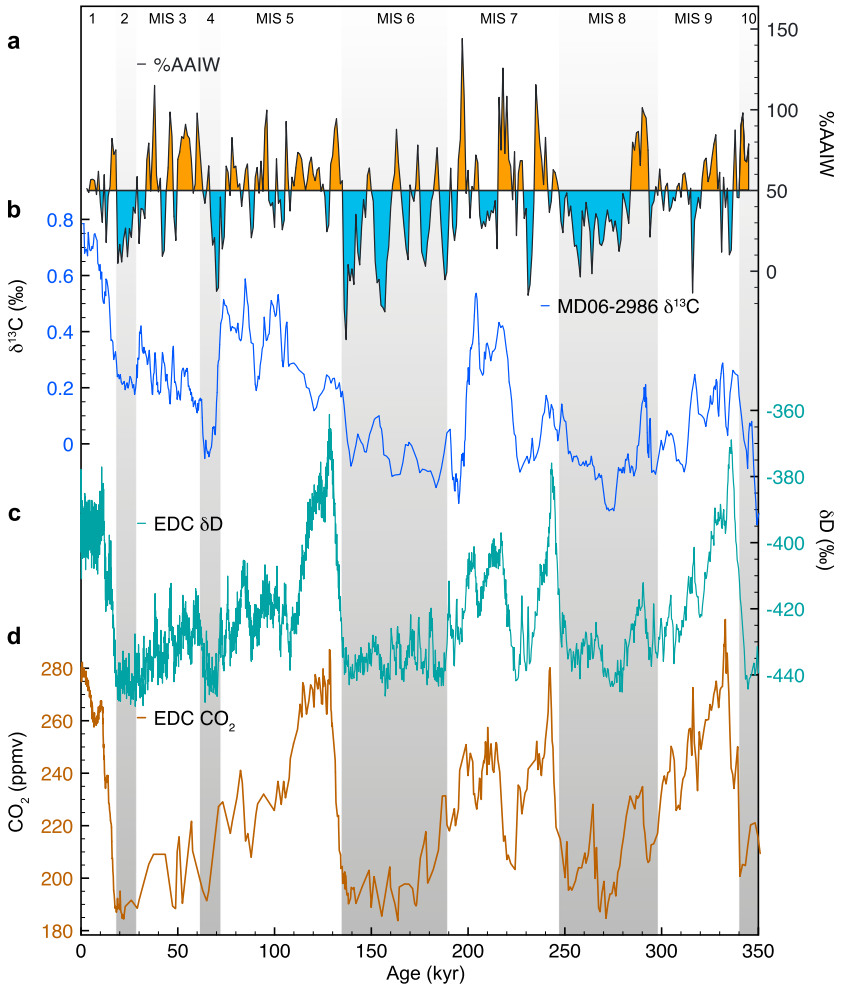

Figure 8. AAIW variability of the southwest Pacific compared to Antarctic ice core records over the past 350,000 years. (a) %AAIW (black) as an indicator for the presence/absence of AAIW in MD97-2120. Orange peaks indicate the presence of AAIW and blue peaks the presence of UCDW. Values higher than 100% and lower than 0% might derive from the comparison of Tasman Sea AAIW to SO-AAIW. (b) Five-point running average benthic (*C. wuellerstorfi*) $\delta^{13}C$ record of Tasman Sea core MD06-2986 (blue). (c) EPICA dome C δD-curve on the AICC2012 timescale (teal) [*Bazin et al.*, 2013; *Jouzel et al.*, 2007; *Veres et al.*, 2013]. (d) Composite CO_2 curve for the last 350 kyr (brown; 0–22 kyr: EPICA Dome C, [*Monnin et al.*, 2001] and 22–350 kyr: Vostok, [*Pépin et al.*, 2001; *Petit et al.*, 1999; *Raynaud et al.*, 2005]. Grey shadings as shown in Figure 3.

and MD06-2986 display lower averages with 0.65‰ and 0.3‰, respectively. The isotopic offset between MD06-2990/SO136-003 and MD97-2120 ($\Delta\delta^{13}C_{2990-2120}$) increases during glacials (MIS 6 and MIS 8) from interglacial values of 0.29‰ to a $\Delta\delta^{13}C_{2990-2120}$ of 0.54‰ (Figure 8b).

The comparison of sediment cores above and below MD97-2120 suggests an upward displacement of the AAIW-UCDW interface, locating MD97-2120 in poorer ventilated UCDW during the LGM, MIS 4, MIS 6, and MIS 8. These findings are supported by the analysis of the CDW oxygen minimum, which was found at substantially shallower water depths throughout the LGM [*Hayward et al.*, 2004]. Today older and CO_2 enriched deep waters, like UCDW, are, in general, more corrosive than intermediate waters. Therefore, the findings of *Pahnke et al.* [2003a] who observed increased carbonate dissolution in MD97-2120 throughout cold periods furthermore argues for the presence of corrosive UCDW during glacial periods.

Less pronounced than the AAIW to UCDW shift displayed in the $\delta^{13}C$ record of MD97-2120, the $\delta^{18}O$ record shows a similar shift from low-salinity, higher-temperature AAIW during warmer climatic periods to higher saline and/or lower temperature UCDW during glacial maxima like the LGM or MIS 4 (Figure 3).

The similarity of benthic $\delta^{13}C$ patterns in our cores over the last three glacial-interglacial cycles suggests that source water preformed nutrient changes of AAIW or changes in temperature-dependent fractionation during air-sea gas exchange in the convection region [*Broecker and Maier-Reimer*, 1992] are negligible.

4.1. Proposed Mechanisms

During glacial stages, the boundary, separating high-nutrient (low $\delta^{13}C$) and CO_2 rich waters from a better ventilated and low-nutrient water mass rises from ~2000 m (interglacials and interstadials) to a depth shallower than 1200 m. This shift could be attributed to several factors: A northward displacement of the AAIW source region, end-member $\delta^{13}C$ depletion, increased stratification, decreased biological productivity, increased UCDW upwelling, a reduction in the formation of SO AAIW as proposed by *Bostock et al.* [2004] and *Pahnke and Zahn* [2005], Carbon Isotope Minimum Events (CIMEs) or reduced AAIW subduction due to increased buoyancy.

During the LGM, the winter sea ice surrounding Antarctica advanced to about the position of the modern Polar Front (PF) [*Gersonde et al.,* 2005]. This advance was accompanied by a northward displacement of Antarctic cold waters, where the strongest cooling occurred within the modern Subantarctic Zone (SAZ) [*Gersonde et al.,* 2005]. According to some authors [e.g., *Gersonde et al.,* 2003; *Kohfeld et al.,* 2013; *Sikes et al.,* 2009], the major oceanic fronts as well advanced toward the north, expanding the surface area of the Southern Ocean. As AAIW is closely associated with Subantarctic Mode Water (SAMW) [*Bostock et al.,* 2004] and SAMW in turn is coupled to the SAF [*Hanawa and Talley*, 2001], the upward displacement of the AAIW-UCDW interface could be assigned to a northward displacement of the SAF during the LGM. This process would cause SAMW/AAIW to be subducted further to the north (in relation to warmer intervals) extending only to shallower depths at the core locations analyzed in this study. However, *Hayward et al.* [2008] showed that, in the region off New Zealand, neither the SAF nor the Subtropical Front shifted during glacial/interglacial cycles, due to topographic constraints by the Campbell Plateau and the Chatham Rise, respectively (Figure 1). Therefore, we assume a northward shift of the formation region of SO AAIW south of New Zealand [*Bostock et al.,* 2013a] as an unlikely process to explain the upward displacement of UCDW.

A decline of air-sea exchange during glacials due to the northward expansion of sea ice [*Gersonde et al.,* 2005] and/or an equatorward shift in SWW [e.g., *Mohtadi and Hebbeln*, 2004; *Stuut and Lamy*, 2004] could have depleted the $\delta^{13}C$ due to reduced thermodynamic fractionation in the source region of AAIW [*Mackensen*, 2012]. However, as our intermediate water records show a similar glacial drop in $\delta^{13}C$ as the UCDW records, we propose that this process did not play the dominant role in driving the $\delta^{13}C$ pattern in MD97-2120. Increased upper ocean stratification has the potential to lower the $\delta^{13}C$ level of a water mass by its separation from high $\delta^{13}C$ surface waters. Radiocarbon analyses on cores south of the Chatham Rise indeed constrain a pronounced stratification of the glacial southwest Pacific [*Sikes et al.,* 2000], but place the cline, which separates poorly ventilated waters from overlying waters, below the AAIW at a depth of $>$2000 m. Therefore, a stratified upper ocean cannot explain the low glacial $\delta^{13}C$. However, mixing with $\delta^{13}C$-depleted waters below the cline cannot be excluded.

The preferential uptake of isotopically lighter ^{12}C through biological productivity based on photosynthesis [*Farquhar et al.,* 1989] enriches the $\delta^{13}C_{DIC}$ (dissolved inorganic carbon) in a surface water mass. A decrease in biological export production [*Francois et al.,* 1997] in the formation area of AAIW would therefore decrease the $\delta^{13}C_{DIC}$ in source waters. Although this process cannot be completely excluded, we argue it to be unlikely as *Hayward et al.* [2004] report increased biological productivity in the SAZ off New Zealand. The Phytodetritus Effect [*Mackensen et al.,* 2000] on the other hand has the potential to decrease the $\delta^{13}C$ in epibenthic foraminifera. However, as we mentioned in the results, we assume that our sediment cores were not affected by a pronounced input of organic carbon.

Pahnke and Zahn [2005] already discussed the process of increased UCDW upwelling as a possible explanation for the very low glacial $\delta^{13}C$ values. This process, being in agreement with the $\delta^{13}C$ data [*Pahnke and Zahn*, 2005; this study], could in general explain the isotopic pattern observed in MD97-2120. However, several studies point to decreased glacial upwelling [*Boyle and Keigwin*, 1982; *Sigman and Boyle*, 2000] and ventilation [*Sikes et al.,* 2000; *Skinner et al.,* 2010]. Even though increased upwelling cannot be completely ruled out, we consider this scenario as relatively unlikely.

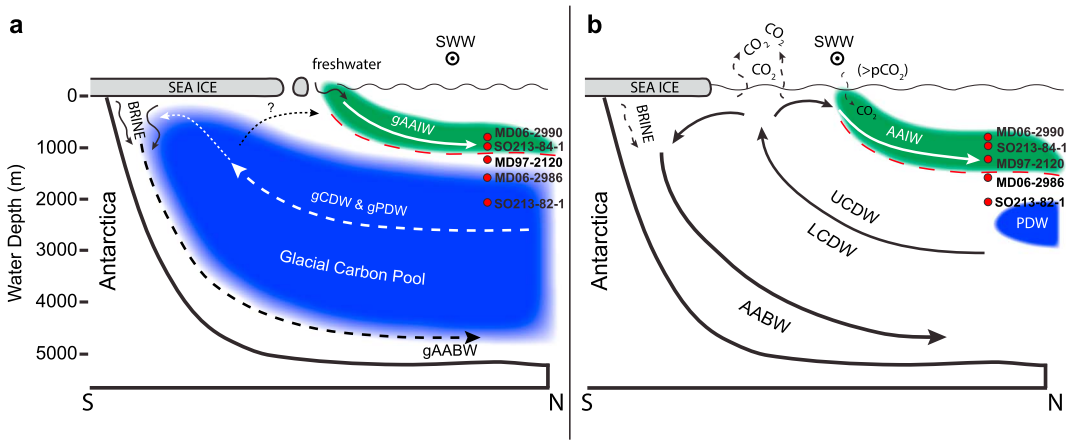

Figure 9. Conceptual schemes of SW Pacific water mass structures. (a) Glacial pattern: Associated with advancing winter sea ice, the Southern Westerly Winds (SWW; dotted circle) shift toward the north, away from the formation region of glacial (g) AAIW (green shaded area). Freshwater input from the close sea ice edge enhances gAAIW buoyancy, locating it above the depth of reference core MD97-2120. The blue-shaded area indicates the old [e.g., *Sikes et al.*, 2000] glacial deep-water carbon pool, rich in CO_2 and nutrients (low $\delta^{13}C$). During glacial maxima, the AAIW/UCDW interface (red dashed line) shifts above 1200 m, bathing the reference core location of MD97-2120 in low $\delta^{13}C$ gUCDW. Dashed arrows indicate a more sluggish deep-water circulation than during interglacial times. Red dots show the modern water depth of sediment cores analyzed in this study. (b) Interglacial pattern: During the warmer stages like the Holocene, the sea ice-derived meltwater input in AAIW declines, while the SWW shift toward a poleward position. Increased AAIW salinity favors a deepening of the AAIW-UCDW interface. Retreating sea ice enables air-sea gas exchange of upwelled CDW, releasing stored CO_2 toward the atmosphere [e.g., *Marchitto et al.*, 2007; *Rose et al.*, 2010]. During times of high atmospheric partial pressure of CO_2 ($>pCO_2$) like today (due to anthropogenic forcing), CO_2 is being entrained into the ocean interior via AAIW. Thus, today the Southern Ocean acts as a CO_2 sink, while in preindustrial times (and other interglacials), the SO released upwelled CO_2 to the atmosphere [e.g., *Gruber et al.*, 2009]. Thick, continuous arrows indicate enhanced ventilation, water mass circulation, and exchange compared to glacial maxima. The old Pacific Deep Water (PDW) carbon pool diminishes and retreats toward its modern dimension [see *Key et al.*, 2004].

Noteworthy features of several intermediate and mode water records at the onset of glacial terminations are pronounced CIMEs [*Curry and Crowley*, 1987; *Ninnemann and Charles*, 1997; *Spero and Lea*, 2002; *Ziegler et al.,* 2013]. A CIME is caused by the reallocation of old (low $\delta^{13}C$) and CO_2-rich waters from the deep Southern Ocean toward the surface by a breakdown in water mass stratification [*Spero and Lea*, 2002; *Ziegler et al.,* 2013]. The incorporation of these old deep waters into the upper water levels ultimately causes the observed CIMEs [*Spero and Lea*, 2002]. As *Spero and Lea* [2002] point out, the deep waters should display an uninterrupted increase in $\delta^{13}C$ throughout a CIME. However, as the deep water $\delta^{13}C$ in MD06-2986 clearly equals the trend of $\delta^{13}C$ in MD97-2120, we argue that the low $\delta^{13}C$ values in MD97-2120 do not display the reallocation of old carbon via upwelling during a CIME, but that the very same water mass (UCDW) influenced both sediment cores. Additionally, the fact that CIMEs are relatively short lived [*Spero and Lea*, 2002] argues against this scenario as the driver for the low $\delta^{13}C$ intervals in MD97-2120.

Although the northern Tasman Sea record FR1/97-GC12 (990 m; 23°34′S 153°46′E;) is located close to the core depth of modern AAIW [*Bostock et al.,* 2004], its LGM $\delta^{13}C$ values are as low as the $\delta^{13}C$ of UCDW records MD06-2986 (1477 m) and SO213-82-1 (2066 m). This implies that in the Tasman Sea as well, glacial AAIW (gAAIW) did not reach as deep as during the Holocene. We conclude that despite findings of increased glacial AAIW formation [*Herguera et al.,* 2010; *Martínez-Méndez et al.,* 2013; *Meissner et al.,* 2005], southern sourced AAIW in the southwest Pacific may not always have reached the core depth of FR1/97-GC12 during the LGM. As *Ribbe* [2001] suggested, the production of AAIW is closely coupled to the wind stress applied on subantarctic surface waters. He showed that the volume of transported AAIW is in direct proportion to the forcing of southern hemispheric wind stresses. During glacial peak times, the northward displacement of SWW [*Mohtadi and Hebbeln*, 2004; *Moreno et al.,* 1999; *Stuut and Lamy*, 2004; *Toggweiler et al.,* 2006] in combination with static oceanic fronts [*Hayward et al.,* 2008] led to a reduction of wind stress in the formation area of SW Pacific AAIW. In addition, the advancing winter sea ice edge increased the glacial import of freshwater by melting sea ice into the AAIW [e.g., *Saenko and Weaver*, 2001] and thereby intensified the SAZ salinity anomaly [*Gersonde et al.,* 2003; *Jenkins*, 1999; *Pahnke and Zahn*, 2005], ultimately hampering the

subduction of AAIW (Figure 9). Furthermore, highly saline bottom waters, stabilized by brine rejection [*Adkins*, 2013] increased the water column density gradient and thus supported the positive buoyancy of fresher AAIW. A salinity-controlled pattern, leading to shallower penetration of glacial AAIW, is also supported by our CCSM3 model runs (Figure 5) that point to an increased density gradient between glacial water masses (Figure S2). In combination, the processes described here might have significantly reduced the downward extension of AAIW within the southwest Pacific. This void, created by the diminishing influence of glacial AAIW was then filled by an upward displacement of underlying UCDW. We visualized the alternation between AAIW and UCDW by calculating the %AAIW at the core depth of MD97-2120, following the approach of *Raymo et al.* [1990] (Figure 8a; supporting information). %AAIW values higher than 50% indicate the presence of AAIW, values lower than 50% the presence of UCDW at the core location of MD97-2120. At the end of each glacial cycle, the low δ^{13}C of MD06-2990/SO136-003/SO213-84-1 and MD97-2120 increase and approach the same absolute values, while simultaneously, UCDW δ^{13}C of SO213-82-1 and MD06-2986 rises just as rapid (Figure 4). Increasing temperatures in the Southern Hemisphere [e.g., *Parrenin et al.,* 2013] reverse the sequence of glacial processes outlined above. Sea ice retreats and therefore reduces the SAZ freshwater anomaly, the SWW shift toward a poleward position, ultimately increasing the subduction, formation and ventilation of deep and intermediate waters [*Toggweiler et al.,* 2006].

The good correlation between atmospheric CO_2, δD, and UCDW δ^{13}C and %AAIW (Figure 8) suggests a close coupling of increased deep water ventilation, AAIW formation, and global climate driven by Southern Hemisphere climatic events.

Pahnke and Zahn [2005] proposed that a transient buoyancy inertia caused by meltwater export, delayed the ventilation of AAIW, as their sea surface temperatures (SSTs) of sediment core MD97-2120 lead the increasing δ^{13}C trend by 1–3 kyr. However, we argue that the lead/lag of MD97-2120 δ^{13}C/SST$_{Mg/Ca}$ is not a consequence of delayed ventilation but of a delayed downward expansion of AAIW and decelerated UCDW ventilation. As already proposed, the enhanced import of meltwater likely led to a buoyancy gain of recently formed AAIW. Only upon a reduction of freshwater input would the AAIW be able to advance to depths greater than about 1200 m. Although the AAIW ventilation occurred at the onset of rising temperatures, the UCDW lagged behind, due to the pool of old and CO_2-rich water that had to be ventilated as shown by *Skinner et al.* [2010].

We further speculate that changes in the AAIW freshwater budget might cause global reorganizations in the oceanic Themohaline Circulation (THC). *Saenko et al.* [2003] showed that the end-member freshwater budget of the THC controls the density gradients of AAIW and North Atlantic Deep Water (NADW) and therefore their formation rate. Freshwater input in one hemisphere can significantly alter the AAIW-NADW density gradient, enhancing, or hampering the formation rate of the respective water mass in the opposing hemisphere [*Weaver et al.,* 2003].

Radiocarbon analyses on planktic and benthic foraminifera proved the presence of exceptional old waters within glacial CDW in the southwest Pacific and South Atlantic [*Sikes et al.,* 2000; *Skinner et al.,* 2010]. At the onset of the most recent deglaciation, deep water ventilation improved simultaneously with the increase in AAIW subduction, outlined above. The restart of the Southern Ocean Meridional Overturning Circulation [*Sigman et al.,* 2010] conveyed ancient CO_2 from the deep ocean toward the surface and ultimately to the atmosphere. During this process of upwelling and the subsequent formation of intermediate waters, the incomplete air-sea gas exchange favored the incorporation of ^{14}C-depleted old waters in AAIW (MD97-2120) during Heinrich Stadial 1 [*Rose et al.,* 2010]. In this context a radiocarbon-based analysis of MD97-2120 during the last glacial would contribute to the results discussed above, as we expect the ^{14}C values of MD97-2120 to decrease as well in intervals marked by the presence of weakly ventilated δ^{13}C- and ^{14}C-depleted UCDW.

5. Conclusions

Recent benthic δ^{13}C and δ^{18}O records from the Bounty Trough and the Tasman Sea off New Zealand allow new insights into the formation and extent of SW Pacific AAIW over the last 350 kyr. The new proxy data and modeling results presented in this study question the hypothesis that stronger water column

stratification resulted in reduced production of glacial AAIW [*Pahnke and Zahn*, 2005]. Our results suggest that a northward displacement of the winter sea ice edge [*Gersonde et al.,* 2005] led to a significantly shallower AAIW subduction in the SW Pacific during glacial maxima. Warmer climatic conditions on the other hand favor the enhanced downward extent of AAIW (Figure 9).

Following the synchronous timing of these observations and published SSTs [*Pahnke and Zahn*, 2005], we conclude that pronounced climate changes in the Southern Hemisphere are the dominating factor, driving changes in AAIW formation, its vertical expansion as well as the ventilation and the associated carbon storage and cycling of CDW.

Vast amounts of anthropogenic CO_2 are transported toward the deep ocean via the AAIW [*Downes et al.,* 2010; *Murata et al.,* 2007, 2010; *Sabine et al.,* 2004], while at the same time stored CO_2 is upwelled within CDW [*Gruber et al.,* 2009] (Figure 9). As model predictions suggest, the current CO_2 sink of the Southern Ocean [*Gruber et al.,* 2009] might evolve into a source due to the poleward shift of SWW and the accompanying increase in CDW upwelling [*Le Quéré et al.,* 2007]. Additional modeling studies [*Downes et al.,* 2010; *Manabe and Stouffer*, 1993] showed that this process might be reversed on longer timescales, leading to increased ocean stratification and decreased AAIW formation and consequently to a reduction in the uptake of anthropogenic CO_2. Thus, in order to specify the Southern Ocean's role in the carbon cycle of a changing climate system, improved insight in this highly dynamic system is essential.

Acknowledgments
This work was funded by the Federal Ministry of Education and Research (BMBF; Germany) project 03G0213A–SOPATRA and the Alfred Wegener Institute, Helmholtz Centre for Polar and Marine Research. We thank captains, crews, and scientific parties of R/V *Sonne* cruise SO213/2 and R/V *Marion Dufresne* cruise MD152 for their support during sample collection; K. Pahnke and A. Sturm for data; A. Mackensen and J. Wollenburg for discussion; R. Fröhlking, N. Lensch, G. Meyer, L. Ritzenhoven. L. Schönborn, M. Seebeck, R. Sieger, and S. Wiebe for technical support. Special thanks goes to H. Bostock, R. Zahn, and C. Charles, for their constructive comments that helped to improve the final version of this manuscript. Data are accessible at http://doi.pangaea.de/10.1594/PANGAEA.835498.

References

Adkins, J. F. (2013), The role of deep ocean circulation in setting glacial climates, *Paleoceanography*, *28*, 539–561, doi:10.1002/palo.20046.
Antonov, J. I., D. Seidov, T. P. Boyer, R. A. Locarnini, A. V. Mishonov, H. E. Garcia, O. K. Baranova, M. M. Zweng, and D. R. Johnson (2010), in *World Ocean Atlas 2009*, Salinity, NOAA Atlas NESDIS 69, vol. 2, edited by S. Levitus, NOAA, U.S. Government Printing Office, Washington, D. C.
Basak, C., E. E. Martin, K. Horikawa, and T. M. Marchitto (2010), Southern Ocean source of ^{14}C-depleted carbon in the North Pacific Ocean during the last deglaciation, *Nat. Geosci.*, *3*, 770–773.
Bazin, L., et al. (2013), An optimized multi-proxy, multi-site Antarctic ice and gas orbital chronology (AICC2012): 120–800 ka, *Clim. Past*, *9*, 1715–1731.
Bostock, H. C., B. N. Opdyke, M. K. Gagan, and L. K. Fifield (2004), Carbon isotope evidence for changes in Antarctic Intermediate Water circulation and ocean ventilation in the southwest Pacific during the last deglaciation, *Paleoceanography*, *19*, PA4013, doi:10.1029/2004PA001047.
Bostock, H. C., B. N. Opdyke, and M. J. M. Williams (2010), Characterising the intermediate depth waters of the Pacific Ocean using δ^{13}C and other geochemical tracers, *Deep Sea Res., Part I*, *57*, 847–859.
Bostock, H. C., P. J. Sutton, M. J. M. Williams, and B. N. Opdyke (2013a), Reviewing the circulation and mixing of Antarctic Intermediate Water in the South Pacific using evidence from geochemical tracers and Argo float trajectories, *Deep Sea Res., Part I*, *73*, 84–98.
Bostock, H. C., et al. (2013b), A review of the Australian-New Zealand sector of the Southern Ocean over the last 30 ka (Aus-INTIMATE project), *Quat. Sci. Rev.*, *74*, 35–57.
Boyle, E. A., and L. D. Keigwin (1982), Deep circulation of the North Atlantic over the last 200,000 years: Geochemical evidence, *Science*, *218*, 784–787.
Broecker, W. S., and E. Maier-Reimer (1992), The influence of air and sea exchange on the carbon isotope distribution in the sea, *Global Biogeochem. Cycles*, *6*, 315–320, doi:10.1029/92GB01672.
Bryan, S. P., T. M. Marchitto, and S. J. Lehman (2010), The release of ^{14}C-depleted carbon from the deep ocean during the last deglaciation: Evidence from the Arabian Sea, *Earth Planet. Sci. Lett.*, *298*, 244–254.
Callahan, J. E. (1972), The structure and circulation of deep water in the Antarctic, *Deep Sea Res.*, *19*, 563–575.
Carter, L., and I. N. McCave (1997), The sedimentary regime beneath the deep western boundary current inflow to the Southwest Pacific Ocean, *J. Sediment. Res.*, *67*(6), 1005–1017.
Carter, L., and J. Wilkin (1999), Abyssal circulation around New Zealand—A comparison between observations and a global circulation model, *Mar. Geol.*, *159*, 221–239.
Carter, L., I. N. McCave, and M. J. M. Williams (2009), Circulation and water masses of the Southern Ocean: A review, in *Developments in Earth and Environmental Science Series. Antarctic Climate Evolution*, edited by F. Florindo and G. Siegert, chap. 4, pp. 85–114, Elsevier, Oxford.
Collins, W. D., et al. (2006), The Community Climate System Model Version 3 (CCSM3), *J. Clim.*, *19*, 2122–2143.
Crundwell, M., G. Scott, T. Naish, and L. Carter (2008), Glacial–interglacial ocean climate variability from planktonic foraminifera during the Mid-Pleistocene transition in the temperate Southwest Pacific, ODP site 1123, *Palaeogeogr. Palaeoclimatol. Palaeoecol.*, *260*, 202–229.
Curry, W. B., and T. J. Crowley (1987), The δ^{13}C of equatorial Atlantic surface waters: Implications for ice age pCO_2 levels, *Paleoceanography*, *2*, 489–517, doi:10.1029/PA002i005p00489.
Downes, S. M., N. L. Bindoff, and S. R. Rintoul (2010), Changes in the subduction of Southern Ocean water masses at the end of the twenty-first century in eight IPCC Models, *J. Clim.*, *23*, 6526–6541.
Duplessy, J.-C., N. J. Shackleton, R. G. Fairbanks, L. Labeyrie, D. Oppo, and N. Kallel (1988), Deepwater source variations during the last climate cycle and their impact on global deepwater circulation, *Paleoceanography*, *3*, 343–360, doi:10.1029/PA003i003p00343.
Emiliani, C. (1955), Pleistocene temperatures, *J. Geol.*, *63*, 538–578.
Epstein, S., and T. Mayeda (1953), Variation of O^{18} content of waters from natura sources, *Geochim. Cosmochim. Acta*, *4*, 213–224.
Farquhar, G. D., J. R. Ehleringer, and K. T. Hubick (1989), Carbon isotope discrimination and photosynthesis, *Annu. Rev. Plant Physiol. Plant Mol. Biol.*, *40*, 503–537.
Francois, R., M. A. Altabet, E.-F. Yu, D. M. Sigman, M. B. Bacon, M. Frank, G. Bohrmann, G. Bareille, and L. D. Labeyrie (1997), Contribution of Southern Ocean surface-water stratification to low atmospheric CO_2 concentrations during the last glacial period, *Nature*, *389*, 929–935.

Gersonde, R., et al. (2003), Last glacial sea surface temperatures and sea-ice extent in the Southern Ocean (Atlantic-Indian sector): A multiproxy approach, *Paleoceanography*, *18*(3), 1061, doi:10.1029/2002PA000809.
Gersonde, R., X. Crosta, A. Abelmann, and L. Armand (2005), Sea-surface temperature and sea ice distribution of the Southern Ocean at the EPILOG Last Glacial Maximum—A circum-Antarctic view based on siliceous microfossil records, *Quat. Sci. Rev.*, *24*, 869–896.
Gruber, N., et al. (2009), Oceanic sources and sinks of atmospheric CO_2, *Global Biogeochem. Cycles*, *23*, GB1005, doi:10.1029/2008GB003349.
Hanawa, K., and L. D. Talley (2001), Mode waters, in *Ocean Circulation and Climate*, edited by G. Siedler, J. Church, and J. Gould, pp. 373–386, Academic, San Diego, Calif.
Hayward, B. W., H. L. Neil, R. Carter, H. R. Grenfell, and J. J. Hayward (2002), Factors influencing the distribution patterns of recent deep-sea benthic foraminifera, east of New Zealand, Southwest Pacific Ocean, *Mar. Micropaleontol.*, *46*, 139–176.
Hayward, B. W., A. T. Sabaa, and H. R. Grenfell (2004), Benthic foraminifera and the late Quaternary (last 150 ka) paleoceanographic and sedimentary history of the Bounty Trough, east of New Zealand, *Palaeogeogr. Palaeoclimatol. Palaeoecol.*, *211*, 59–92.
Hayward, B. W., et al. (2008), The effect of submerged plateaux on Pleistocene gyral circulation and sea-surface temperatures in the Southwest Pacific, *Global Planet. Change*, *63*, 309–316.
Heath, R. A. (1981), Oceanic fronts around southern New Zealand, *Deep Sea Res. A*, *28*(6), 547–560.
Heath, R. A. (1985), A review of the physical oceanography of the seas around New Zealand—1982, *N. Z. J. Mar. Freshwater Res.*, *19*, 79–124.
Herguera, J. C., T. Herbert, M. Kashgarian, and C. Charles (2010), Intermediate and deep water mass distribution in the Pacific during the Last Glacial Maximum inferred from oxygen and carbon stable isotopes, *Quat. Sci. Rev.*, *29*, 1228–1245.
Jenkins, A. (1999), The impact of melting ice on ocean waters, *J. Phys. Oceanogr.*, *29*, 2370–2381.
Jouzel, J., et al. (2007), Orbital and millennial antarctic climate variability over the past 800,000 years, *Science*, *317*, 793–796.
Key, R. M., A. Kozyr, C. L. Sabine, K. Lee, R. Wanninkhof, J. L. Bullister, R. A. Feely, F. J. Millero, C. Mordy, and T.-H. Peng (2004), A global ocean carbon climatology: Results from Global Data Analysis Project (GLODAP), *Global Biogeochem. Cycles*, *18*, GB4031, doi:10.1029/2004GB002247.
Kohfeld, K. E., R. M. Graham, A. M. de Boer, L. C. Sime, E. W. Wolff, C. Le Quéré, and L. Bopp (2013), Southern Hemisphere westerly wind changes during the Last Glacial Maximum: Paleo-data synthesis, *Quat. Sci. Rev.*, *68*, 76–95.
Kroopnick, P. M. (1985), The distribution of ^{13}C of ΣCO_2 in the world oceans, *Deep Sea Res.*, *32*(1), 57–84.
Le Quéré, C., et al. (2007), Saturation of the Southern Ocean CO_2 sink due to recent climate change, *Science*, *316*, 1735–1738.
Mackensen, A. (2012), Strong thermodynamic imprint on recent bottom-water and epibenthic $\delta^{13}C$ in the Weddell Sea revealed: Implications for glacial Southern Ocean ventilation, *Earth Planet. Sci. Lett.*, *317–318*, 20–26.
Mackensen, A., H.-W. Hubberton, T. Bickert, G. Fischer, and D. K. Fütterer (1993), The $\delta^{13}C$ in benthic foraminiferal tests of *Fontbotia wuellerstorfi* (Schwager) relative to the $\delta^{13}C$ of dissolved inorganic carbon in southern ocean deep water: Implications for glacial ocean circulation models, *Paleoceanography*, *8*, 587–610, doi:10.1029/93PA01291.
Mackensen, A., S. Schumacher, J. Radke, and D. N. Schmidt (2000), Microhabitat preferences and stable carbon isotopes of endobenthic foraminifera: Clue to quantitative reconstruction of oceanic new production?, *Mar. Micropaleontol.*, *40*, 233–258.
Mackensen, A., M. Rudolph, and G. Kuhn (2001), Late Pleistocene deep-water circulation in the subantarctic eastern Atlantic, *Global Planet. Change*, *30*, 197–229.
Manabe, S., and R. J. Stouffer (1993), Century-scale effects of increased atmospheric CO_2 on the ocean-atmosphere sytem, *Nature*, *364*, 215.
Marchitto, T. M., S. J. Lehman, J. D. Ortiz, J. Flückinger, and A. van Geen (2007), Marine radiocarbon evidence for the mechanism of deglacial atmospheric CO_2 rise, *Science*, *316*, 1456–1459.
Martínez-Méndez, G., D. Hebbeln, M. Mohtadi, F. Lamy, R. De Pol-Holz, D. Reyes-Macaya, and T. Freudenthal (2013), Changes in the advection of Antarctic Intermediate Water to the northern Chilean coast during the last 970 kyr, *Paleoceanography*, *28*, 607–618, doi:10.1002/palo.20047.
McCartney, M. S. (1977), Subantarctic mode water, in *A Voyage of Discovery: George Deacon 70th Anniversary Volume*, Supplement to Deep-Sea Research and Oceanographic Abstracts, edited by M. V. Angel, pp. 103–119, Pergamon Press, Oxford.
McCave, I. N., and L. Carter (1997), Recent sedimentation beneath the Deep Western Boundary Current off northern New Zealand, *Deep Sea Res., Part I*, *44*(7), 1203–1237.
McCave, I. N., L. Carter, and I. R. Hall (2008), Glacial-interglacial changes in water mass structure and flow in the SW Pacific Ocean, *Quat. Sci. Rev.*, *27*, 1886–1908.
Meissner, K. J., E. D. Galbraith, and C. Völker (2005), Denitrification under glacial and interglacial conditions: A physical approach, *Paleoceanography*, *20*, PA3001, doi:10.1029/2004PA001083.
Merkel, U., M. Prange, and M. Schulz (2010), ENSO variability and teleconnections during glacial climates, *Quat. Sci. Rev.*, *29*, 86–100.
Mohtadi, M., and D. Hebbeln (2004), Mechanisms and variations of the paleoproductivity off northern Chile (24°S–33°S) during the last 40,000 years, *Paleoceanography*, *19*, PA2023, doi:10.1029/2004PA001003.
Monnin, E., A. Indermühle, A. Dällenbach, J. Flückiger, B. Stauffer, T. F. Stocker, D. Raynaud, and J.-M. Barnola (2001), Atmospheric CO_2 concentrations over the last glacial termination, *Science*, *291*, 112–114.
Moreno, P. I., T. V. Lowell, G. L. Jacobson, and G. H. Denton (1999), Abrupt vegetation and climate changes during the Last Glacial Maximum and last termination in the Chilean Lake District: A case study from Canal de la Puntilla (41°S), *Geogr. Ann., Ser. A*, *81*, 285–311.
Murata, A., Y. Kumamoto, S. Watanabe, and M. Fukasawa (2007), Decadal increases of anthropogenic CO_2 in the South Pacific subtropical ocean along 32°S, *J. Geophys. Res.*, *112*, C05033, doi:10.1029/2005JC003405.
Murata, A., Y. Kumamoto, K. Sasaki, S. Watanabe, and M. Fukasawa (2010), Decadal increases in anthropogenic CO_2 along 20°S in the South Indian Ocean, *J. Geophys. Res.*, *115*, C12055, doi:10.1029/2010JC006250.
Ninnemann, U., and C. D. Charles (1997), Regional differences in quaternary subantarctic nutrient cycling: Link to intermediate and deep water ventilation, *Paleoceanography*, *12*, 560–567, doi:10.1029/97PA01032.
Orsi, A. H., T. Whitworth III, and W. D. Nowlin Jr. (1995), On the meridional extent and fronts of the Antarctic Circumpolar Current, *Deep Sea Res., Part I*, *42*(5), 641–673.
Pahnke, K., and R. Zahn (2005), Southern Hemisphere water mass conversion linked with North Atlantic climate variability, *Science*, *307*, 1741–1746.
Pahnke, K., R. Zahn, H. Elderfield, and M. Schulz (2003a), 340,000-year centennial-scale marine record of Southern Hemisphere climatic oscillation, *Science*, *301*, 948–952.
Pahnke, K., R. Zahn, H. Elderfield, and M. Schulz (2003b), 340,000-Year centennial-scale marine record of Southern Hemisphere climatic oscillation supplements, *Science*, doi:10.1126/science.1084451.
Parrenin, F., V. Masson-Delmotte, P. Köhler, D. Raynaud, D. Paillard, J. Schwander, C. Barbante, A. Landais, A. Wegner, and J. Jouzel (2013), Synchronous change of atmospheric CO_2 and Antarctic temperature during the last deglacial warming, *Science*, *339*, 1060–1063.

Pépin, L., D. Raynaud, J.-M. Barnola, and M. F. Loutre (2001), Hemispheric roles of climate forcings during glacial-interglacial transitions as deduced from the Vostok record and LLN-2D model experiments, *J. Geophys. Res.*, *106*, 31,885–31,892, doi:10.1029/2001JD900117.
Peterson, C. D., L. E. Lisiecki, and J. V. Stern (2014), Deglacial whole-ocean $\delta^{13}C$ change estimated from 480 benthic foraminiferal records, *Paleoceanography*, *29*, 549–563, doi:10.1002/2013PA002552.
Petit, J. R., et al. (1999), Climate and atmospheric history of the past 420,000 years from the Vostok ice core, Antarctica, *Nature*, *399*, 429–436.
Proust, J.-N., G. Lamarche, S. Migeon, and H. L. Neil (2006), Geoscience Cruise, MD152/MATACORE (24 January-7 February 2006) on R/V Marion-Dufresne, Tectonic and climatic controls on sediment budget, *Rep.*, 107 pp., Institut polaire français Paul-Émile Victor.
Raymo, M. E., W. F. Ruddiman, N. J. Shackleton, and D. Oppo (1990), Evolution of Atlantic-Pacific $\delta^{13}C$ gradients over the last 2.5 m.y., *Earth Planet. Sci. Lett.*, *97*, 353–368.
Raynaud, D., J.-M. Barnola, R. Souchez, R. Lorrain, J.-R. Petit, P. Duval, and V. Y. Lipenkov (2005), Palaeoclimatology: The record for marine isotopic stage 11, *Nature*, *436*, 39–40.
Ribbe, J. (2001), Intermediate water mass production controlled by Southern Hemisphere winds, *Geophys. Res. Lett.*, *28*, 535–538, doi:10.1029/2000GL012242.
Rintoul, S. R., C. Hughes, and D. Olbers (2001), The Antarctic circumpolar current system, in *Ocean, Ice and Atmosphere: Interactions at the Antarctic Continental Margin*, edited by G. Siedler, J. Church, and J. Gould, pp. 151–171, Academic Press, San Diego, London.
Rojas, M., P. Moreno, M. Kageyama, M. Crucifix, C. Hewitt, A. Abe-Ouchi, R. Ohgaito, E. C. Brady, and P. Hope (2009), The Southern Westerlies during the last glacial maximum in PMIP2 simulations, *Clim. Dyn.*, *32*, 525–548.
Rose, K. A., E. L. Sikes, T. P. Guilderson, P. Shane, T. M. Hill, R. Zahn, and H. J. Spero (2010), Upper-ocean-to-atmosphere radiocarbon offsets imply fast deglacial carbon dioxide release, *Nature*, *466*, 1093–1097.
Sabine, C. L., et al. (2004), The oceanic sink for anthropogenic CO_2, *Science*, *305*, 367–371.
Saenko, O. A., and A. J. Weaver (2001), Importance of wind-driven sea ice motion for the formation of Antarctic Intermediate Water in a global climate model, *Geophys. Res. Lett.*, *28*, 4147–4150, doi:10.1029/2001GL013632.
Saenko, O. A., A. J. Weaver, and J. M. Gregory (2003), On the link between the two modes of the ocean thermohaline circulation and the formation of global-scale water masses, *J. Clim.*, *16*(16), 2797–2801.
Schmitz, W. J. (1995), On the interbasin-scale thermohaline circulation, *Rev. Geophys.*, *33*, 151–173, doi:10.1029/95RG00879.
Shackleton, N. J. (1977), The oxygen isotope stratigraphic record of the Late Pleistocene, *Philos. Trans. R. Soc. B*, *280*, 169–182.
Shackleton, N. J., and N. D. Opdyke (1973), Oxygen isotope and palaeomagnetic stratigraphy of Equatorial Pacific core V28-238: Oxygen isotope temperatures and ice volumes on a 10^5 year and 10^6 year scale, *Quat. Res.*, *3*, 39–55.
Sigman, D. M., and E. A. Boyle (2000), Glacial/interglacial variations in atmospheric carbon dioxide, *Nature*, *407*, 859–869.
Sigman, D. M., M. P. Hain, and G. H. Haug (2010), The polar ocean and glacial cycles in atmospheric CO_2 concentration, *Nature*, *466*, 47–55.
Sikes, E. L., C. R. Samson, T. P. Gullderson, and W. R. Howard (2000), Old radiocarbon ages in the southwest Pacifc Ocean during the last glacial period and deglaciation, *Nature*, *405*, 555–559.
Sikes, E. L., W. R. Howard, C. R. Samson, T. S. Mahan, L. G. Robertson, and J. K. Volkman (2009), Southern Ocean seasonal temperature and subtropical Front movement on the South Tasman Rise in the late Quaternary, *Paleoceanography*, *24*, PA2201, doi:10.1029/2008PA001659.
Skinner, L. C., S. Fallon, C. Waelbroeck, E. Michel, and S. Barker (2010), Ventilation of the deep Southern Ocean and deglacial CO_2 rise, *Science*, *328*, 1147–1151.
Sloyan, B. M., L. D. Talley, T. K. Chereskin, R. A. Fine, and J. Holte (2010), Antarctic Intermediate Water and Subantarctic Mode Water formation in the Southeast Pacific: The Role of turbulent mixing, *J. Phys. Oceanogr.*, *40*, 1558–1574.
Spero, H. J., and D. W. Lea (2002), The cause of carbon isotope minimum events on glacial terminations, *Science*, *296*, 522–525.
Stein, R. (1991), Accumulation of organic carbon in marine sediments, in *Lecture Notes in Earth Sciences*, edited by S. Bhattacharji et al., pp. 217, Springer, Berlin.
Stott, L. D., J. Southon, A. Timmermann, and A. Koutavas (2009), Radiocarbon age anomaly at intermediate water depth in the Pacific Ocean during the last deglaciation, *Paleoceanography*, *24*, PA2223, doi:10.1029/2008PA001690.
Stuut, J.-B. W., and F. Lamy (2004), Climate variability at the southern boundaries of the Namib (southwestern Africa) and Atacama (northern Chile) coastal deserts during the last 120,000 yr, *Quat. Res.*, *62*, 301–309.
Sutton, P. J. H. (2003), The Southland Current: A subantarctic current, *N. Z. J. Mar. Freshwater Res.*, *37*, 645–652.
Thiede, J. (1999), FS Sonne-Fahrtbericht SO136, cruise report SO136-TASQWA: Quaternary variability of water masses in Southern Tasman sea and the southern ocean (sw pacific sector); Wellington-Hobart, October 16-November 12, *Rep.*, 106 pp., GEOMAR, Kiel.
Tiedemann, R. (2012), FS Sonne Fahrtbericht / Cruise Report SO213, *Rep.*, Alfred Wegener Institute, Bremerhaven.
Toggweiler, J. R., K. Dixon, and W. Broecker (1991), The Peru upwelling and the ventilation of the South Pacific thermocline, *J. Geophys. Res.*, *96*, 20,467–20,497, doi:10.1029/91JC02063.
Toggweiler, J. R., J. L. Russell, and S. R. Carson (2006), Midlatitude westerlies, atmospheric CO_2, and climate change during the ice ages, *Paleoceanography*, *21*, PA2005, doi:10.1029/2005PA001154.
Tomczak, M., and J. S. Godfrey (1994), *Regional Oceanography: An Introduction*, 382 pp., Pergamon, Oxford.
Varma, V., M. Prange, F. Lamy, U. Merkel, and M. Schulz (2011), Solar-forced shifts of the Southern Hemisphere Westerlies during the Holocene, *Clim. Past*, *7*, 339–347.
Veres, D., et al. (2013), The Antarctic ice core chronology (AICC2012): An optimized thousand years multi-parameter and multi-site dating approach for the last 120, *Clim. Past*, *9*, 1733–1748.
Waelbroeck, C., L. Labeyrie, E. Michel, J.-C. Duplessy, J. F. McManus, K. Lambeck, E. Balbon, and M. Labracherie (2002), Sea-level and deep water temperature changes derived from benthic foraminifera isotopic records, *Quat. Sci. Rev.*, *21*, 295–305.
Weaver, A. J., O. A. Saenko, P. U. Clark, and J. X. Mitrovica (2003), Meltwater pulse 1A from Antarctica as a trigger of the Bølling-Allerød warm interval, *Science*, *299*, 1709–1713.
Yeager, S. G., C. A. Shields, W. G. Large, and J. J. Hack (2006), The low-resolution CCSM3, *J. Clim.*, *19*, 2545–2566.
Zahn, R., T. F. Pedersen, B. D. Bornhold, and A. C. Mix (1991), Water mass conversion in the glacial Subarctic Pacific (54°N, 148°W): Physical constraints and the benthic-planktonic stable isotope record, *Paleoceanography*, *6*, 543–560, doi:10.1029/91PA01327.
Ziegler, M., P. Diz, I. R. Hall, and R. Zahn (2013), Millennial-scale changes in atmospheric CO_2 levels linked to the Southern Ocean carbon isotope gradient and dust flux, *Nat. Geosci.*, *6*, 457–461.